MDPI

Article

Leachate Experiments to Evaluate Weathering of Waste Rock for Backfill Aquifers in Restored Coal Mine Pits, Powder River Basin, USA

Julianna Martin and Jeff B. Langman *

Department of Earth and Spatial Sciences, University of Idaho, Moscow, ID 83844, USA
* Correspondence: jlangman@uidaho.edu

Abstract: Restoration of open-pit mines may utilize waste rock for landscape reconstruction, which can include the construction of backfill aquifers. Weathering and contaminant transport may be different in backfill aquifers compared to the surrounding aquifer because of newly available mineral surfaces and transportable nano- to micro-scale particles generated during mining. Waste rock from the Cordero Rojo open-pit coal mine in the Powder River Basin was exposed to benchtop leachate experiments for 20 weeks at temperatures of 5 °C and 20 °C. Collected leachate was analyzed for Eh, pH, specific conductance, alkalinity, and cation and anion concentrations as unfiltered and 0.45-μm and 0.2-μm filtered concentrations. During the experiment, leachate Eh and pH substantially varied during the first 55 days, which corresponds to a period of high specific conductance (>1000 μS/cm) and alkalinity (>200 mg/L). Correspondingly, anion and cation concentrations were the largest during this early weathering stage, and the filter fractions indicated multiple forms of transported elements. After this early weathering stage, column leachate evolved towards a weathering equilibrium of neutral, oxidizing, and low solute conditions indicated by positive Eh values, pH near 7, and specific conductance <500 μS/cm. This evolution was reflected in the decline and stabilization or non-detection of metal(loid) concentrations reflective of a shift to primarily bulk aluminosilicate weathering when coal- and salt-associated elements, such as arsenic, cadmium, and selenium, were not detected or at minimal concentrations. Over the course of the experiment, the solute trend of certain elements indicated particular weathering processes—cadmium and nanoparticle transport, selenium and salt dissolution, and arsenic and pyrite oxidation. The mining of overburden formations and use of the waste rock for backfill aquifers as part of landscape reconstruction will create newly available mineral surfaces and nanoparticles that will weather to produce solute concentrations not typically found in groundwater associated with the original overburden.

Keywords: waste rock; backfill aquifer; leachate experiment; weathering evolution

1. Introduction

A backfill aquifer is produced from the filling of a mine pit with waste rock (e.g., overburden and interburden materials) and the return of groundwater from infiltrating precipitation or lateral inflow from the adjacent aquifer. As water percolates into the waste rock, a reaction front propagates through the aquifer as newly exposed mineral surfaces and small particles (e.g., nanoparticles) are exposed to weathering and transport processes [1,2]. Progression of the reaction front is visible in the temporal evolution of solute release until a new equilibrium of weathering is established [3–6]. The difficulty in predicting the potential water quality of backfill aquifers is not our lack of mineral weathering knowledge but our lack of understanding of the availability of potential sources contributing to solute release and transport in this modified aquifer matrix. The incomplete source identification for the prediction of solute release has resulted in the exceedance of water quality criteria for backfill aquifers when it was predicted that weathering of the waste rock would not result in groundwater contamination issues [7,8].

Backfill aquifers in the Powder River Basin (Figure 1), the largest coal mining district in the United States, have shown variable water quality and exceedance of water quality criteria for metal(loid) and nonmetal contaminants due to the waste rock used for landscape restoration. The blasting and transport of the waste rock produce a new aquifer matrix with the generation of new mineral surfaces and nanoparticles that can produce high weathering and solute transport rates [5,9–11]. A weathering or release rate is the rate at which primary minerals are congruently or incongruently transformed into secondary minerals with the release of dissolved reaction products (solutes) [9]. Predicting the release of solutes can be difficult because of coupled and sustained biogeochemical processes, but the identification of potential solute sources and associated reaction rates with the development of an applicable conceptual model is critical for estimating solute release and evaluating future water quality [12–14]. A governing physical property of weathering is the available surface area where smaller grain fractions typically undergo the greatest weathering and release of solutes [15–17]. The generation and transport of nanoparticles, materials with at least one dimension within the nanometer scale [18], can also contribute to the solute load through inclusion in the dissolved phase (<0.45-µm filtering) and will weather to produce additional solutes during transport [19]. Using waste rock from the Cordero Rojo Mine in the Powder River Basin (PRB), a leach column experiment was conducted to discriminate solute sources from newly created mineral surfaces and transportable particles to better understand solute release during early-stage weathering that can impact the water quality of backfill aquifers. Leachate data provided insight into the mineral sources of the solutes and the form of the solutes released with the weathering of the waste rock.
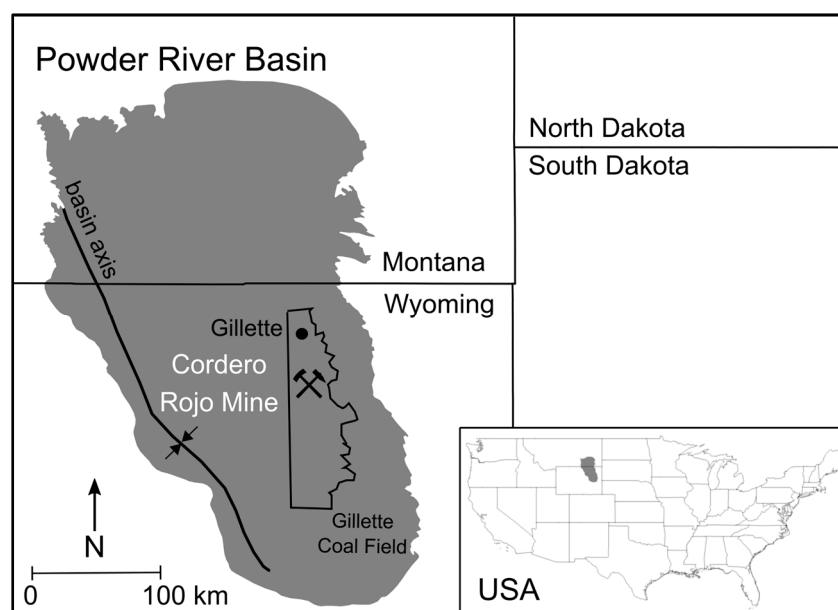

Figure 1. Location of the Cordero Rojo Mine near the town of Gillette in the Powder River Basin of Wyoming, USA (basin boundary from the U.S. Geological Survey).

1.1. Powder River Basin Geology

The PRB (Figure 1) is a north-northwest to south-southeast trending asymmetric syncline that accumulated marine, alluvial, fluvial, and lacustrine sediments [20]. The structural axis is located along the western part of the basin (Figure 1). The western limb of the PRB is characterized by steeply dipping (~20°) strata, and the eastern limb is characterized by gently dipping (2–5°) strata, including the coal-bearing rocks [21]. The Cordero Rojo Mine extracts its coal from the Wyodak-Anderson coal seam of the Tongue River member of the Fort Union Formation, which is overlain by upper units of the Paleocene Fort Union Formation and the near-surface Eocene Wasatch Formation [22] (Figure 2). Open-pit mining of the coal takes advantage of the near-surface coal deposits

along the basin's eastern margin and their gentle westward dip. A typical PRB mining operation consists of a westward-moving open pit, removal of overburden and coal, nearby storage of waste rock, and landscape restoration to the east of the active mine site (Figure 3).
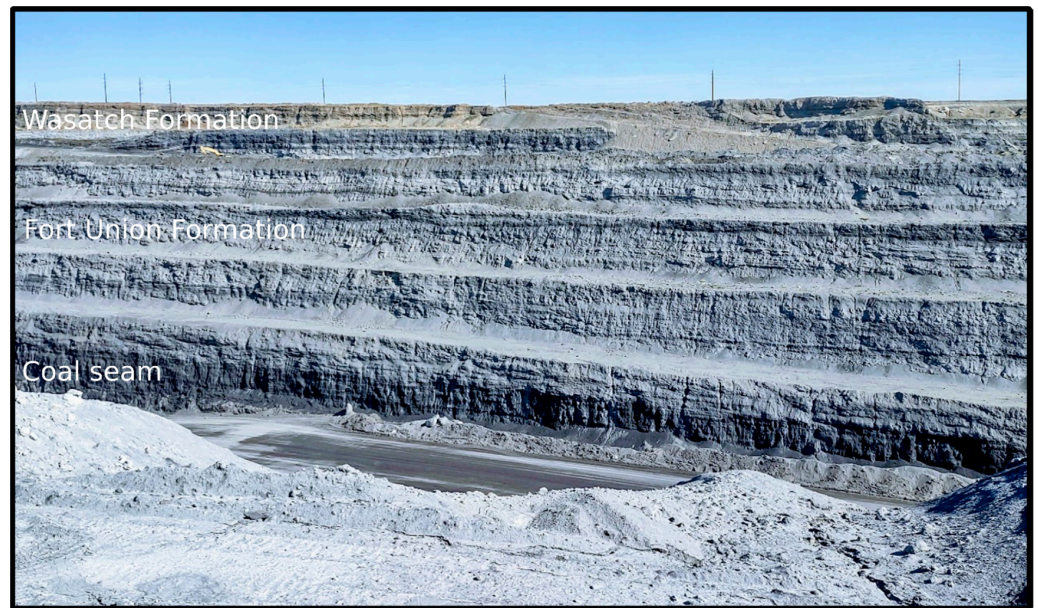

Figure 2. Overburden and coal seam at the Cordero Rojo Mine, Powder River Basin, Wyoming, USA.

Figure 3. Removal of overburden and waste rock generation during open-pit coal mining at the Cordero Rojo Mine, Powder River Basin, Wyoming, USA.

1.2. Powder River Basin Waste Rock and Groundwater Contaminants

Waste rock from the Cordero Rojo Mine in the PRB is derived from the Wasatch and Fort Union formations—sequences of interbedded fluvial, lacustrine, and palustrine deposits that compose the overburden [23–25]. The Wasatch Formation is composed of sandstones, mudstones, conglomerate lenses, and interbedded limestone and evaporites [26]. The Fort Union Formation is composed of non-sulfidic shales, mudstones, and concretionary sandstones [27,28] whose paleoenvironment also produced the interbedded

low-sulfur coal [29–31]. The PRB coal contains accessory minerals, such as arsenic-bearing pyrite [FeS$_2$], cadmium-bearing sphalerite [(Zn,Fe)S], and galena [PbS] [32]. Primary contaminants (exceedance of water quality criteria) detected in backfill aquifers of the PRB include arsenic [As], barium [Ba], manganese [Mn], and selenium [Se] [33]. Such contamination is not typically found in groundwater that has interacted with the Wasatch and Fort Union formations [34]. Therefore, it was hypothesized that production and disposal of the waste rock have incorporated small coal particles containing higher concentrations of the potential contaminants, exposed previously unavailable forms of the contaminants (e.g., bound salts), and/or produced contaminant-containing nanoparticles that are weathered and transported within the backfill aquifers. The goal of this study was to discriminate contaminant sources through the interpretation of solute trends indicative of weathering processes in the waste rock.

2. Study Methods

2.1. Waste Rock Collection

Wasatch and Fort Union waste rock were collected within two weeks of initial excavation from the Cordero Rojo Mine in August of 2021. The waste rock samples were collected from the most recent waste piles generated with mining of the overburden (nearest waste piles to the active mine site, as shown in Figure 3). Sample collection was completed according to the "clean hands" techniques as prescribed for field and laboratory experiments involving trace metals [35,36]. Wasatch and Fort Union waste rock were segregated during the mining process, and samples were collected separately per standard practice for sampling aggregates [37]. The samples were screened in the field to <6.3 mm to meet the criteria for kinetic columns [38,39]. The 300 kg of screened waste rock (86 kg Wasatch waste rock and 214 kg Fort Union waste rock) was sealed in 0.02 m^3 buckets and transported to the University of Idaho, where the waste rock was temporarily stored at 5 °C until dried at 125 °C for 48 h.

2.2. Waste Rock Characterization

To distinguish potential formation differences in contaminant sources, the dried Wasatch and Fort Union waste rock were evaluated for element composition (X-ray fluorescence (XRF)), grain size distribution, weathering resistance (slake durability test [40]), and surface area (Brunauer–Emmett–Teller (BET) analysis) prior to the start of the leach column experiment. Wasatch and Fort Union waste rock were submitted to the Washington State University GeoAnalytical Laboratory for XRF analysis (Advant'XP + sequential XRF, fused beads). Grain size distribution and slake durability tests were performed at the University of Idaho. Surface area was analyzed by a contract laboratory using a TriStar II Plus High Throughput Surface Area and Porosity Analyzer.

2.3. Leach Columns

A 20-week leach column experiment was conducted to evaluate the weathering processes responsible for controlling the release and transport of potential contaminants from the waste rock. Warm-room (20 °C ± 1 °C) and cold-room (5 °C ± 0.5 °C) PVC columns (0.6 m (H) × 0.1 m (W)) were loaded with 0.8 kg of dried Wasatch waste rock and 3.2 kg of dried Fort Union waste rock to mimic overburden distributions at the Cordero Rojo Mine, which is replicated with backfill aquifer construction. The base of each column contained a two-layer, 2.5-cm thick, non-reactive mesh filter for the retention of the waste rock material while allowing for the passage of <10-μm particles into the upper portion of the mesh and <4-μm particles in the lower portion of the mesh. This dual-layer mesh assisted in retaining bulk solids in the column while minimizing the clogging of the system with the movement of microparticles into the mesh.

The weathering cycle for each leach column consisted of a semiweekly schedule of the drip introduction of 1 L of deionized water and full saturation of the waste rock for 72 h followed by a 2 h drain period and a 6 h unsaturated period before resaturation of

the column. This is a modification of the standard humidity cell protocol [39] to simulate primarily saturated (e.g., aquifer) conditions and allow for the collection of sufficient water volume for analysis of environmental parameters and solutes. The twice-weekly collection of the leachate from each column was immediately analyzed for pH ($\pm$0.01 pH), Eh ($\pm$0.2 mV), and specific conductance ($\pm$0.01 μS/cm) with calibrated Orion 3-Star meters/probes followed by submission of samples to the University of Idaho Analytical Services Laboratory for analysis of anion (0.45-μm filtered) and cation (unfiltered (total), 0.45-μm filtered, and 0.2-μm filtered) concentrations. Additionally, alkalinity was determined by an OrionStarT940 auto-titrator using 0.1 N HCl ($\pm$0.1 mg/L as $CaCO_3$). Filtered anion (bromide [Br], chloride [Cl], fluoride [F], nitrate-nitrite [NO_3-NO_2 as N], ortho-phosphate [PO_4], and sulfate [SO_4]) concentrations were determined via ion chromatography (Dionex Aquion Ion Chromatograph). Cation (aluminum [Al], As, Ba, boron [B], Cd, calcium [Ca], chromium [Cr], copper [Cu], iron [Fe], lead [Pb], magnesium [Mg], Mn, molybdenum [Mo], nickel [Ni], potassium [K], Se, sodium [Na], zinc [Zn]) concentrations of unfiltered and filtered samples were determined via inductively coupled plasma optical emission spectrometry (ICP-OES) for larger concentrations (Perkin Elmer Optima 8300 ICP-OES) and inductively coupled plasma mass spectrometry (ICP-MS) for smaller concentrations (Agilent 7800 ICP-MS). Duplicate samples were randomly collected during each leachate collection period to assess laboratory analysis accuracy.

2.4. Data Analysis

The goal of the data analysis was the evaluation of the temporal trends, or variability with time, of the environmental parameters and of the release of solutes for the identification of substantive changes in weathering processes. The identification of changes in solute release from the waste rock assisted in discriminating contaminant sources and the weathering processes that released the solutes into solution. The temporal trends of the environmental parameters of pH, specific conductance, and alkalinity were smoothed using the moving window average (4-point window) technique to reduce the volatility of the data series and allow for an improved display of the data trends (all data in Supplementary Materials). Values of Eh were not smoothed to preserve reduction–oxidation (redox) conditions that widely varied during the experiment. A principal component analysis (PCA) was used to identify clusters of related metal(loid) solutes for discriminating potential weathering processes in warm and cold conditions and the unfiltered and filter fractions. Solute data sets that were predominantly (>80 %) below laboratory reporting limits were not included in the PCA.

A Spearman rank correlation analysis of Eh and redox-sensitive elements (As, Fe, Mn, and Mo) was performed to evaluate the oxidative dissolution of sulfide minerals, such as pyrite, that are present in the Fort Union Formation [32]. The Spearman test is a nonparametric measure of rank correlation (statistical dependence between the rankings of two variables) that produces a statistic (ρ) between +1 (perfect positive relation) and −1 (perfect negative relation). This correlation analysis was performed using only the warm-room unfiltered and filtered values because of substantial non-detection results for these elements in the cold-room leachate. A false discovery rate (q-value) was used in place of a *p*-value to minimize the presentation of false negatives. Additionally, the activation energy (E_a, Equation (1)) of the oxidative dissolution of pyrite was calculated to evaluate temporal changes in pyrite weathering that may indicate inhibition of sulfide weathering because of precipitate formation [41]. Arsenic was selected for the calculation of the activation energy because of its strong correlation with Eh and the presence of Fe and sulfur [S] in other mineral sources found in the waste rock [42]. The Arrhenius equation of a single temperature and rate constant (Equation (1)) was used to calculate E_a instead of the typical two-temperature/two-rate method because cold-room As concentrations decreased

below detection levels during the experiment. The one-temperature/rate method employs the geometric solution or slope (line of best fit) of the ln k-to-time relation for estimating E_a:

$$\ln(k) = \ln(A) - (E_a/RT) \tag{1}$$

where E_a is the activation energy (J·mol^{-1}), R is the universal gas constant (8.314×10^{-3} J·mol^{-1}·K^{-1}), A is a pre-exponential factor (s^{-1}), and T is the temperature (K) at the respective times of the observed rate constant (k in mol·m^{-2}·s^{-1}).

3. Results and Discussion

3.1. Waste Rock Characterization

Large concentrations of Al and silicon (Si) were present in the Wasatch and Fort Union waste rock, reflective of the dominant aluminosilicate minerals that compose these fluvial and lacustrine deposits [20,26] (Figure 4). Larger concentrations of redox-sensitive elements of Fe and Mn were present in the Fort Union waste rock, which are indicative of the low-energy paleoenvironments associated with certain units of the Fort Union Formation [43,44]. The slake durability tests indicated stronger rock (93% durability index) from the Wasatch Formation compared to a durability index of 89% for rock from the Fort Union Formation. Such results align with the presence of substantial sandstone in the Wasatch Formation [26] compared to the higher content of shales and mudstones in the Fort Union Formation [44]. Correspondingly, the grain size distribution analysis indicated a greater fraction of clay-sized particles (7.6%) present in the Fort Union waste rock. The greater presence of smaller particles in the Fort Union waste rock also translated to a greater surface area of 14.2 m^2/g compared to the 5.1 m^2/g for the Wasatch sample.
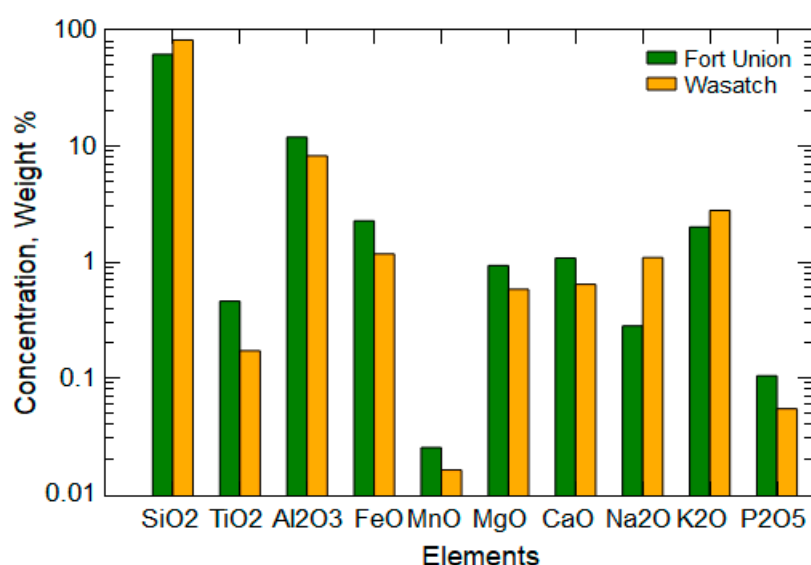

Figure 4. Element composition of the Fort Union and Wasatch waste rock from the Cordero Rojo Mine.

3.2. Leachate Environmental Conditions

The environmental parameters for warm- and cold-room leachates indicated high variability during the first 55 days of the experiment (Figure 5). Eh fluctuated between positive values (maximum of 142 mV for warm-room leachate and 154 mV for cold-room leachate) and negative values (minimum of −113 mV for the warm-room leachate and −118 mV for the cold-room leachate), indicating alternating oxidizing and reducing conditions with the greatest variability during the first 45 days. Specific conductance ranged from 6410 μS/cm to 315 μS/cm for the warm-room leachate and 6350 μS/cm to 271 μS/cm for cold-room leachate, and the specific conductance of leachate from both columns decreased sharply during the first 40 days of the experiment (Figure 5b). Values

of pH remained near neutral for the entire experiment, ranging from 6.05 to 7.03 for the warm-room leachate and 6.47 to 7.04 for the cold-room leachate (Figure 5c). However, comparison of the warm-room and cold-room pH trends indicated a greater difference in pH values during the first 55 days. Alkalinity ranged from 550 mg/L to 148 mg/L for the warm-room leachate and 613 mg/L to 139 mg/L for the cold-room leachate (Figure 5d) with a sharp decline in both alkalinities during the first 20 days and a slower decrease from day 20 to day 70.
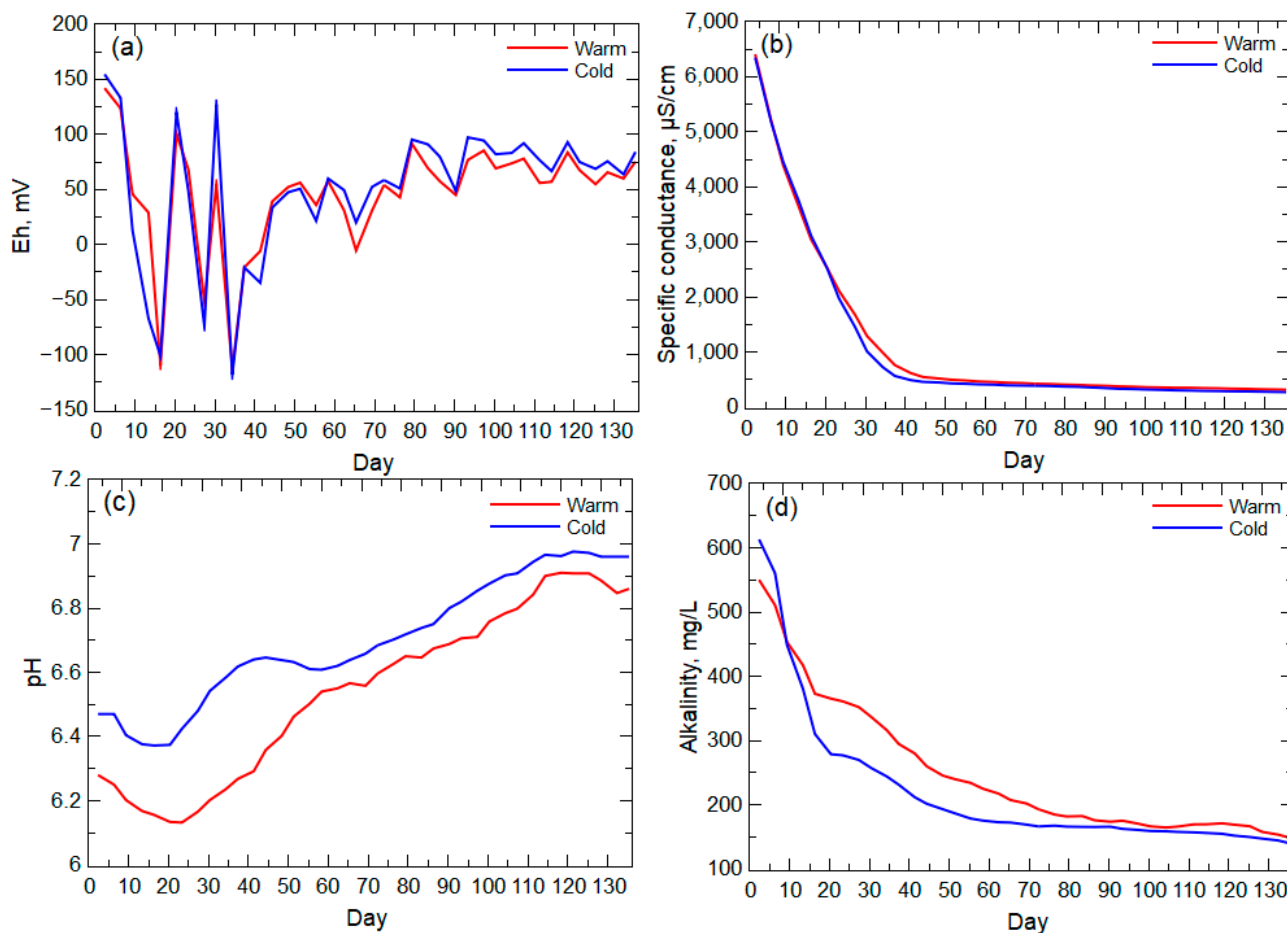

Figure 5. (**a**) Eh, (**b**) specific conductance, (**c**) pH, and (**d**) alkalinity for leachate from the warm- and cold-room columns. All trendlines have been smoothed using the moving window average (4-point window) technique except for Eh.

The high-solute-release period (early weathering stage) indicated by the leachate specific conductance likely is a result of the flushing of nano- to micro-scale particles and the influence of fast reaction weathering, such as sulfide oxidation [11,45], when the largest surface area of these minerals was available. This early weathering stage (day 3 to day 31, specific conductance >1000 µS/cm) also corresponds to sharp decreases and increases in Eh values and the period of maximum pH difference between the warm-room and cold-room leachates (Figure 5). These results indicate oxygen-consuming and acid-generating reactions, such as the oxidative dissolution of pyrite [46]. The lessening of the temperature effect on pH by day 55 corresponds to the stabilization of positive Eh values and the lessening of the decrease in the specific conductance trend (past the inflection point), which indicate a shift to weathering of less reactive minerals (e.g., aluminosilicates) and loss (consumption) of the more reactive sulfide minerals. Alkalinity values in the warm- and cold-room leachates remained elevated past this early weathering stage indicative of the relatively slower reactivity of available carbonate minerals [6,9,47], which have been identified in the Wasatch Formation [26,32].

3.3. Weathering Processes and Solute Trends

The first component (PC1, Table 1) of the PCA indicated an association (covariance of 0.14) of the major cations (Ca, Mg, and K) along with Mn, Ni, and Zn that is consistent in the unfiltered and filtered concentrations in warm- and cold-room conditions (Table 1, bold blue values). This association of the major cations indicates primarily bulk aluminosilicate and carbonate weathering throughout the experiment. The inclusion of Mn and Zn in this associated group likely reflects the presence of Mn and Zn-bearing carbonate species that have been identified in the Powder River Basin overburden formations [32]. Additionally, the Ni likely is from a clay source [32,48,49] that is weathered and transported during the experiment. The association of the redox-sensitive Mn with these elements likely is the result of the weathering of Mn oxides found in the Wasatch Formation [50], which is supported by the lack of correlation (Spearman ρ of -0.04 to -0.03, q-value of 0.84) between Eh and Mn concentrations (unfiltered or filtered) where a correlation would be expected if the Mn was being released with sulfide oxidation. The second component (PC2, Table 1) of the PCA indicated a correlation of As and Fe (stronger in filtered results) likely because of their association in sulfide minerals (e.g., As-bearing pyrite) found in the Wyodak-Anderson coal [48,51]. The second component also indicated an opposing correlation of Mo (positive) and Fe and As (negative) in the warm-room leachate (lack of detectable concentrations in the cold-room leachate), which may indicate the presence of Mo in the coal [52] that has a different mineral source than Fe and As. The association of Mo in PC2 likely is derived from the remaining organic carbon in the coal [32], which is supported by the strong, positive correlation (Spearman's ρ of 0.58 to 0.55, q-value of 0.0009) between Mo and Eh and suggestive of the oxidation of an organic source and release of Mo [53].

Table 1. Covariance matrix of the principal component analysis (two components: PC1 and PC2) for warm- and cold-room solute concentrations for each concentration fraction (total (unfiltered), 0.45-µm filtered, and 0.2 µm filtered). Noted associations in bold and colored fonts.

Element		Warm			Cold		
		Total	**0.45-µm**	**0.2-µm**	**Total**	**0.45-µm**	**0.2-µm**
As	PC1	0.02	0.03	0.03	0.09	0.13	0.13
	PC2	**−0.29**	**−0.26**	**−0.27**	−0.09	0.12	0.13
Ba	PC1	−0.13	−0.13	−0.13	−0.12	−0.13	−0.13
	PC2	0.09	0.09	0.09	0.14	0.14	0.14
B	PC1	0.11	0.14	0.14	0.09	0.14	0.14
	PC2	−0.05	0.01	0.01	0.06	−0.05	−0.05
Ca	PC1	**0.15**	**0.15**	**0.15**	**0.14**	**0.14**	**0.14**
	PC2	0.01	0.01	0.01	−0.03	−0.02	−0.02
Fe	PC1	0.11	0.06	0.07	0.03	−0.06	−0.06
	PC2	**−0.12**	**−0.27**	**−0.26**	0.14	−0.01	−0.01
Mg	PC1	**0.14**	**0.14**	**0.14**	**0.14**	**0.14**	**0.14**
	PC2	0.07	0.07	0.07	0.05	0.05	0.05
Mn	PC1	**0.14**	**0.14**	**0.14**	**0.14**	**0.14**	**0.14**
	PC2	−0.07	−0.07	−0.06	−0.04	−0.01	−0.01
Mo	PC1	−0.02	−0.02	−0.01	0.03	0.03	0.03
	PC2	0.26	0.25	0.27	0.23	0.26	0.26
Ni	PC1	**0.14**	**0.14**	**0.14**	**0.14**	**0.14**	**0.14**
	PC2	0.04	0.05	0.05	0.07	0.08	0.08
K	PC1	**0.14**	**0.14**	**0.14**	**0.14**	**0.14**	**0.14**
	PC2	0.04	0.05	0.05	0.03	0.03	0.03
Zn	PC1	**0.14**	**0.14**	**0.14**	**0.14**	**0.14**	**0.14**
	PC2	0.06	0.04	0.06	0.05	0.04	0.04

3.3.1. Salt Dissolution or Nanoparticle Flushing

The PCA did not include elements that were only detectable in the leachate during the first two weeks of the experiment, such as Cd and Se (Figure 6a,b). These elements

have an association with sulfide minerals in the PRB coal [42,54,55], but their concentration trends did not mimic a release indicative of the oxidative dissolution of pyrite, such as is seen with the As concentrations (Figure 6c). In the overburden formations, Se can be found in coal, coal-associated pyrite, water-leachable salts, and as sorbed particles (e.g., selenite [SeO_3]) [54]. Dreher and Finkelman [56] indicated that Se salts from past oxidation of pyrite may be the primary source of Se in the overburden, although they found seven different forms of Se with no discrimination between Wasatch and Fort Union formations. The quick release of Se and lack of difference between filter fraction concentrations and temperature conditions (Figure 6b) are indicative of a fast-dissolving salt and/or desorption and oxidation of Se particles, such as selenite. The incorporation of Se into gypsum ($CaSO_4$) can occur with the oxidation of pyrite/coal and the substitution of Se for S in gypsum [57,58]. Such processes are partially responsible for the significant presence of gypsum in Powder River Basin sedimentary formations [59–63]. Se-bearing salts can readily dissolve, but the dissolution of the salts may not contribute substantial soluble Se species (e.g., selenate (SeO_4^{2-})) if selenite is produced because of the preference of selenite to readily sorb to sediments [64–66]. The Se released into the leachate appears to be primarily particle release (early and large concentrations) with a contribution from Se salt dissolution that is more visible in the second week when the warm-room leachate indicated higher concentrations of Se.
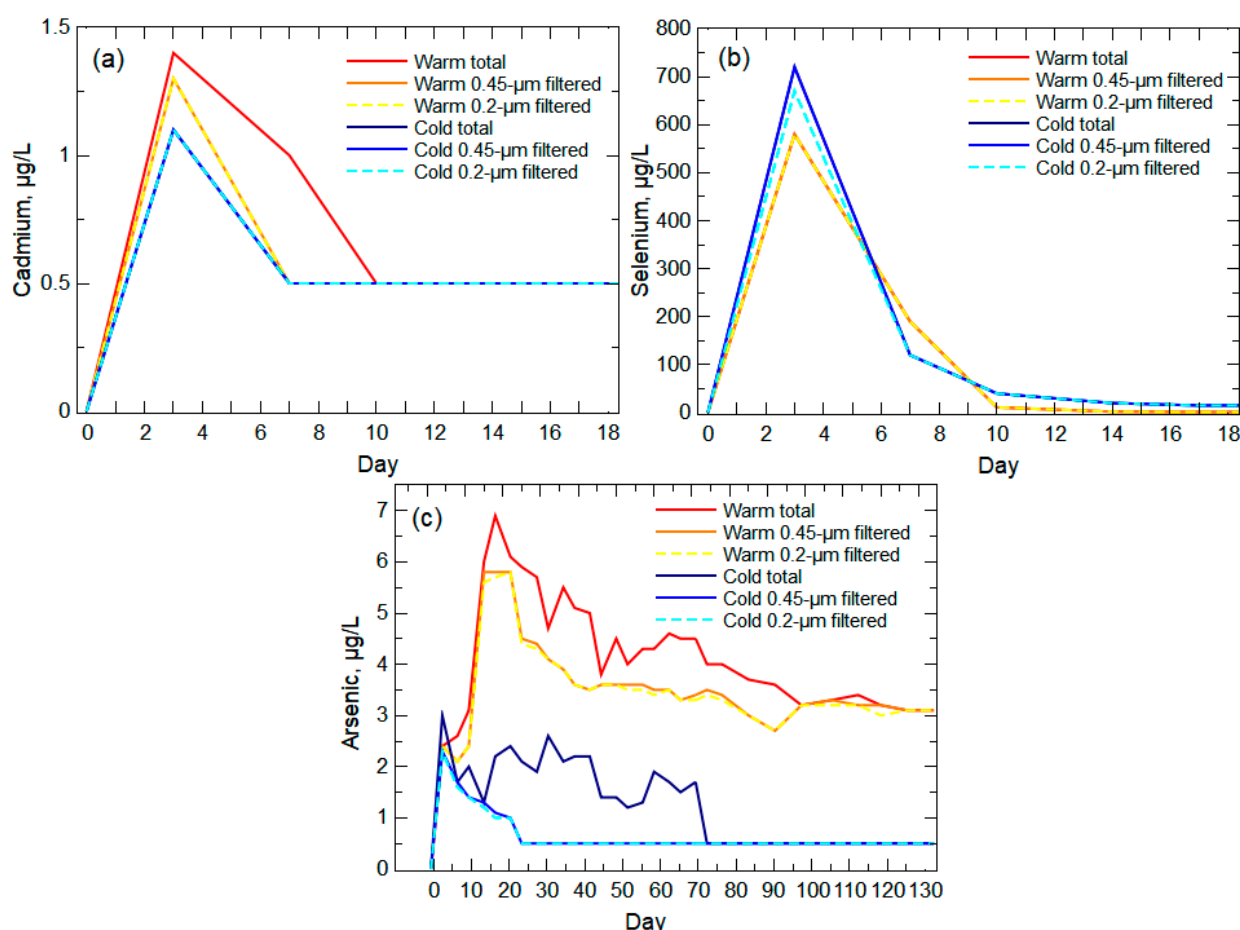

Figure 6. Unfiltered (total) and filtered concentrations in the warm-room and cold-room leachates for (**a**) cadmium and (**b**) selenium during the first 18 days of the experiment and (**c**) arsenic during the entire length of the experiment. All non-detect values were set to 0.5 μg/L, which is half the reporting limit for each of the analytes.

The leachate Cd trends indicate an early concentration peak that quickly decreased after day 3 for all filtered warm- and cold-room results and after day 7 for unfiltered warm-

room concentrations (Figure 6a). Cadmium has not been documented as a salt byproduct from the oxidation of sulfide minerals in the Fort Union Formation, but Cd is associated with sphalerite [(Fe, Zn)S] found in PRB coal [48]. Given the likely presence of Se salts from the oxidation of pyrite, it can be assumed that Cd was similarly released with sphalerite oxidation and deposited in the overburden formations. The introduction of leach water to the waste rock would not have a similar mobilizing effect on Cd compared to Se if both elements are contained in readily dissolvable salts since Cd is less soluble than Se [67]. This lower solubility of Cd is reflected in the much lower concentrations of Cd released from the waste rock compared to Se (Figure 6) even though there are equivalent amounts of Cd and Se in the Wyodak-Anderson coal seam [68]. With the lower solubility of Cd, it is assumed that the early release of Cd from the waste rock is because of the transport of Cd-bearing particles, primarily nanoparticles [69]. Not all of the Cd was present in nanoparticles given the greater release of Cd in the unfiltered warm-room leachate, which indicated a more torturous path of the release of larger particles being transported from the waste rock. Comparison of the pre-experiment Wasatch and Fort Union rock samples to post-experiment samples from the warm-room column indicated the loss of the smallest grains (<0.07 mm) from the Fort Union waste rock during the experiment indicative of the loss (e.g., transport, weathering) of small particles (Figure 7).
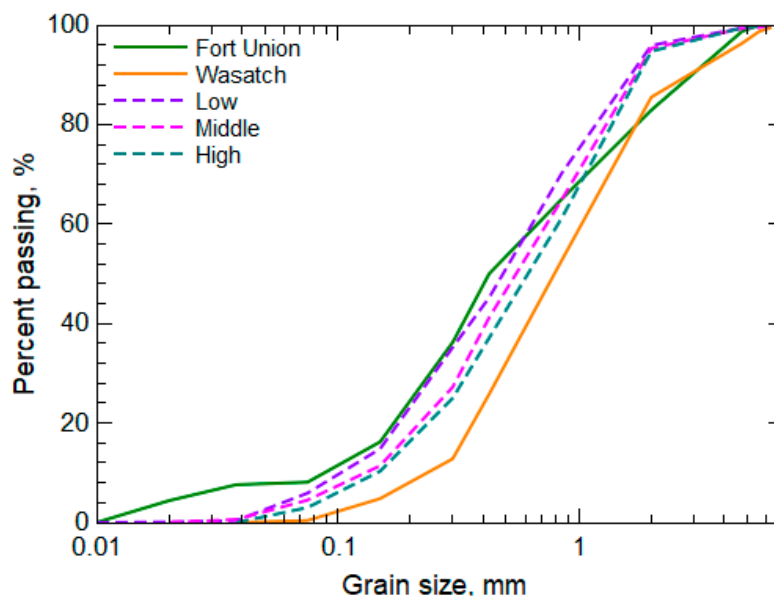

Figure 7. Grain size analysis of waste rock from the pre-experiment Fort Union and Wasatch samples and post-experimental waste rock sampled at three locations from the warm-room leach column (low, middle, and high).

3.3.2. Sulfide Oxidation

Arsenic concentrations were largest in warm-room and cold-room leachates during the early weathering stage when Eh varied between positive and negative values (Figure 6c), reflective of the likely consumption of oxygen with sulfide mineral weathering. The correlation analysis indicated a strong-to-moderate negative correlation (Spearman's ρ of −0.56 to −0.29, q-value of 0.0009 to 0.1) between As and Eh for the filtered and unfiltered concentrations. The majority of the As released in the warm-room leachate was present in the 0.2-μm filtered samples indicating ion release and/or small nanoparticles (Figure 6c). The larger As concentrations in unfiltered leachate from both temperature conditions indicate some release of As-bearing microparticles from the columns. The substantial difference in As concentrations between warm-room and cold-room leachates indicates a temperature effect for oxidative dissolution of As-bearing pyrite. However, the cold-room leachate continued to show the presence of As in the unfiltered solution following the loss of detectable As in the filtered fractions.

The release of As with weathering of As-bearing pyrite typically would result in an early peak concentration because of the dissolution of the source mineral(s) outer layer (rim or coating) followed by a moderated release according to the mass-to-volume ratio of the available mineral source and pH of the porewater solution [70,71]. The primary loss of As from the waste rock during the early weathering stage for the warm-room column is in the filtered samples and displays a concentration trend that peaks near day 17, followed by a moderate decreasing trend. The post-peak trend of As concentrations follows an expected element release trend for the oxidative dissolution of pyrite [72], which is indicative of the weathering of the As-bearing pyrite contained in the PRB coal that was incorporated into the waste rock. Calculation of the effective activation energy of pyrite weathering (Figure 8) from the filtered concentrations of As presents a typical energy trend of an initial energy barrier (oxidation of the mineral surface), an early drop in the energy barrier as the sulfide surface degrades, and a slow increase in the necessary energy for oxidation of the remaining sulfide mineral. This trend represents the oxidation of the unreacted sulfide surface (shrinking core model), which becomes controlled by the inward diffusion of oxygen given the pore-blocking effect of Fe and S precipitates on the unreacted sulfide surface [73]. This oxygen diffusion effect is more pronounced in neutral conditions, in which Fe is not solubilized and can form substantial Fe (oxyhydr)oxide precipitates [74–76]. The effective activation energy trend aligns with the evolution of activation energy necessary for the different bonding arrangements where the initial dissociation of oxygen at the sulfide surface typically requires an activation energy of 22.6 kJ/mol [77] (compared to our calculated 18.2 kJ/mol) followed by lower energy requirements with degradation of the mineral structure.
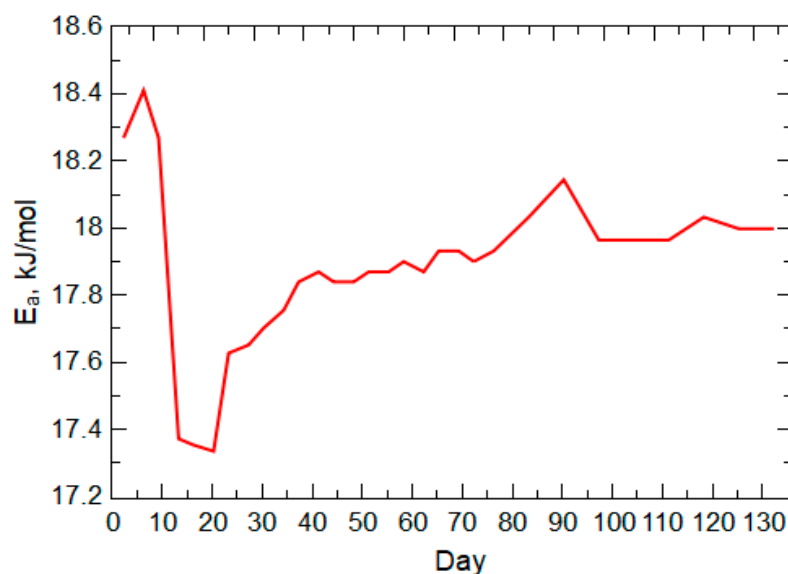

Figure 8. Activation energy (E_a) of pyrite weathering derived from warm-room leach column arsenic concentrations during the 20-week experiment.

3.3.3. Bulk Solid Weathering

With the identification of salt dissolution, particle transport, and pyrite oxidation contributing to the high solute release period, an additional weathering process is necessary to explain the large concentrations in most solutes during the early weathering stage and the following period of higher alkalinity (Figure 5). Transport of other nanoparticles and weathering of the bulk aluminosilicate and carbonate minerals likely explains the remaining contributions to the high solute and high alkalinity periods prior to the waste rock equilibrating to the low-solute weathering period (post-day 70). Carbonates typically weather at a higher rate compared to aluminosilicates [78], which may explain the higher Ca concentrations compared to K (Figure 9) even though there is greater K in the Wasatch and Fort Union waste rock (Figure 4). Carbonate weathering likely is responsible for the

pH moderation (>6.1) during pyrite oxidation early in the experiment and the increasing pH during the remainder of the experiment (Figure 5) as well as the longer period of high alkalinity compared to the high specific conductance period (Figure 5). The large, early concentrations for Ca and K suggest the release of Ca- and K-bearing nanoparticles [19], desorption (exchangeable ions) from larger particles [79], and/or loss from roughened surfaces [80], followed by a typical slow release of these elements with bulk aluminosilicate weathering [81,82]. Warm-room leachate shows higher initial concentrations than cold-room leachate for both Ca and K, which is the result of temperature and pH controls on desorption and mineral degradation [62–67].
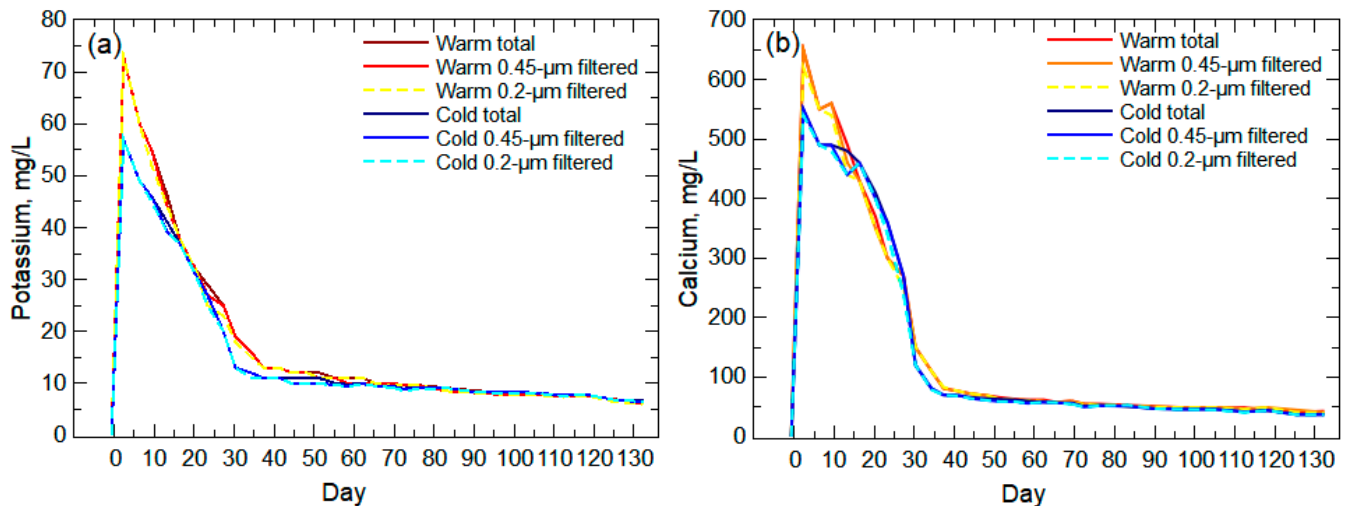

Figure 9. Potassium (**a**) and calcium (**b**) unfiltered (total) and filtered concentrations for the warm-room and cold-room leachates during the 20-week leach column experiment.

3.3.4. Multiple Source Weathering

Iron concentrations for warm- and cold-room leachates indicated multiple weathering processes causing the release of Fe over the course of the experiment (Figure 10). Iron content in the Wasatch and Fort Union waste rock is substantial (Figure 4) and has multiple mineral sources, including sulfides (pyrite) and aluminosilicates (feldspars and associated clays) along with sorbed Fe (oxyhydr)oxide particles. The relation of Fe and Eh was a moderate-to-weak negative correlation (Spearman's ρ of −0.31 for the filtered concentrations (q-value of 0.01) and −0.11 for the unfiltered concentrations (q-value of 0.7)), likely because of the variety of Fe sources and solubility controls on Fe. Given the low solubility of Fe^{3+} in oxidizing and near-neutral waters [83,84], Fe likely was released from the waste rock as desorbed Fe (oxyhydr)oxide particles early in the experiment, which accounts for the large total Fe concentration peak at day 3. The potential for mobile Fe forms is a complex interaction of environmental conditions and solute composition and concentrations that commonly results in the formation of nanoscale to colloidal Fe particles [85–89]. The much larger concentration of Fe in the warm-room leachate during this first week of the experiment is indicative of the effect of pH and temperature on Fe particle desorption and transport [90–92]. After the initial peak of Fe, there is a substantial release of Fe from the warm-room leachate with oxidation of the pyrite, which is limited under the cold-room conditions [93]. As Fe forms are mobilized and removed from the waste rock, along with the lessening of available sulfide surfaces, Fe starts to weather at a consistent and lower release rate at approximately day 65 (Figure 10), similar to the trends of Ca and K (Figure 9). This Fe trend likely is the result of the release of Fe (oxyhydr)oxides with weathering of the bulk solids and continued desorption and particle aggregation/deaggregation [94,95].
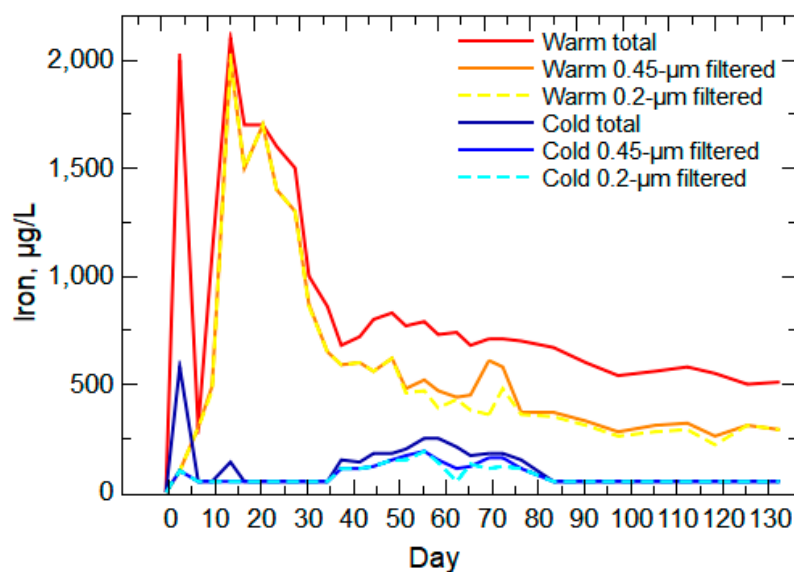
Figure 10. Iron unfiltered (total) and filtered concentrations for warm-room and cold-room leachates during the 20-week leach column experiment. Non-detect values were set to half the reporting limit (50 μg/L).

4. Conclusions

During mine site restoration, the construction and saturation of backfill aquifers may cause groundwater quality impacts because of freshly exposed mineral surfaces and the presence of newly created and transportable particles in the waste rock. Monitoring of groundwater in backfill aquifers of the Powder River Basin has indicated water quality impacts that were not expected given groundwater quality in aquifers contained in the original overburden/waste rock formations. A 20-week leach column experiment was conducted to characterize solute sources and weathering processes for recently generated waste rock from the Cordero Rojo Mine in the Powder River Basin. Analysis of the Eh, pH, specific conductance, alkalinity, and cation and anion concentrations of the leachate collected from warm-room and cold-room columns indicated an early weathering stage during the first 55 days of the experiment—indicated by Eh alternating between positive and negative values, pH < 6.5, specific conductance up to 6500 μS/cm, alkalinity > 500 mg/L, and the largest anion and cation concentrations during this period. After this early weathering period, alkalinity decreased but remained elevated at 200 to 300 mg/L and, along with elevated calcium values, indicated a transitional stage of additional carbonate weathering. Following this transitional weathering period, a low solute period representative of primarily aluminosilicate weathering occurred after day 70.

Multiple weathering processes were identified from leachate solute trends—particle transport, salt dissolution, sulfide oxidation, carbonate dissolution, and the weathering of the bulk aluminosilicate matrix. Certain elements indicated one or two weathering processes that were primarily responsible for the release of an element into solution: cadmium from particle transport during early flushing, selenium from particle transport and salt dissolution with early flushing and weathering of highly soluble minerals, arsenic from oxidation of pyrite found in the coal, calcium from particle transport and carbonate dissolution during and after the early weathering period, and potassium from particle transport and aluminosilicate weathering from early flushing through to equilibrium weathering. Elements with multiple mineral sources, such as iron, produced complex concentration trends because of concurrent and sequential weathering processes. The mining and landscape restoration process produces newly exposed mineral surfaces and nano- to micro-scale particles that may be weathered and transported in groundwater, creating water quality issues not expected given historical aquifer water quality in the regional geology of the Powder River Basin. Mining companies should expect an early weathering stage in back-

fill aquifers where contaminant concentrations may be higher unless actions are taken to minimize the presence or availability of newly accessible contaminant sources in the waste rock.

References

1. Sharma, V.K.; Filip, J.; Zboril, R.; Varma, R.S. Natural Inorganic Nanoparticles—Formation, Fate, and Toxicity in the Environment. *Chem. Soc. Rev.* **2015**, *44*, 8410–8423. [CrossRef]
2. Jun, Y.-S.; Lee, B.; Waychunas, G.A. In Situ Observations of Nanoparticle Early Development Kinetics at Mineral−Water Interfaces. *Environ. Sci. Technol.* **2010**, *44*, 8182–8189. [CrossRef] [PubMed]
3. Acero, P.; Ayora, C.; Carrera, J.; Saaltink, M.W.; Olivella, S. Multiphase Flow and Reactive Transport Model in Vadose Tailings. *Appl. Geochem.* **2009**, *24*, 1238–1250. [CrossRef]
4. Blowes, D.W.; Jambor, J.L. The Pore-Water Geochemistry and the Mineralogy of the Vadose Zone of Sulfide Tailings, Waite Amulet, Quebec, Canada. *Appl. Geochem.* **1990**, *5*, 327–346. [CrossRef]
5. Dosseto, A.; Turner, S.P.; Chappell, J. The Evolution of Weathering Profiles through Time: New Insights from Uranium-Series Isotopes. *Earth Planet. Sci. Lett.* **2008**, *274*, 359–371. [CrossRef]
6. Yoo, K.; Mudd, S.M. Discrepancy between Mineral Residence Time and Soil Age: Implications for the Interpretation of Chemical Weathering Rates. *Geology* **2008**, *36*, 35–38. [CrossRef]
7. Slagle, S.E.; Lewis, B.D.; Lee, R.W. *Ground-Water Resources and Potential Hydrologic Effects of Surface Coal Mining in the Northern Powder River Basin, Southeastern Montana*; Water Supply Paper; U.S. Geological Survey: Reston, VA, USA, 1985. [CrossRef]
8. Bartos, T.T.; Ogle, K.M. *Water Quality and Environmental Isotopic Analyses of Ground-Water Samples Collected from the Wasatch and Fort Union Formations in Areas of Coalbed Methane Development: Implications to Recharge and Ground-Water Flow, Eastern Powder River Basin, Wyoming*; Water Resources Investigations Report 02-4045; U.S. Geological Survey: Reston, VA, USA, 2002. [CrossRef]
9. Colman, S.M. Rock-Weathering Rates as Functions of Time. *Quat. Res.* **1981**, *15*, 250–264. [CrossRef]
10. Drever, J.I.; Clow, D.W. Weathering Rates in Catchments. In *Reviews in Mineralogy and Geochemistry*; White, A.F., Brantley, S.L., Eds.; Mineralogical Society of America: Chantilly, VA, USA, 1995; Volume 31, pp. 463–483.
11. St-Arnault, M.; Vriens, B.; Blaskovich, R.; Aranda, C.; Klein, B.; Ulrich Mayer, K.; Beckie, R.D. Geochemical and Mineralogical Assessment of Reactivity in a Full-Scale Heterogeneous Waste-Rock Pile. *Miner. Eng.* **2020**, *145*, 106089. [CrossRef]
12. Futter, M.N.; Klaminder, J.; Lucas, R.W.; Laudon, H.; Köhler, S.J. Uncertainty in Silicate Mineral Weathering Rate Estimates: Source Partitioning and Policy Implications. *Environ. Res. Lett.* **2012**, *7*, 024025. [CrossRef]
13. Malmström, M.E.; Destouni, G.; Banwart, S.A.; Strömberg, B.H.E. Resolving the Scale-Dependence of Mineral Weathering Rates. *Environ. Sci. Technol.* **2000**, *34*, 1375–1378. [CrossRef]
14. Salmon, S.U.; Malmström, M.E. Quantification of Mineral Dissolution Rates and Applicability of Rate Laws: Laboratory Studies of Mill Tailings. *Appl. Geochem.* **2006**, *21*, 269–288. [CrossRef]
15. Banwart, S.A.; Evans, K.A.; Croxford, S. Predicting Mineral Weathering Rates at Field Scale for Mine Water Risk Assessment. *Geol. Soc. Lond. Spec. Publ.* **2002**, *198*, 137–157. [CrossRef]
16. Malmström, M.; Banwart, S. Biotite Dissolution at 25 °C: The pH Dependence of Dissolution Rate and Stoichiometry. *Geochim. Cosmochim. Acta* **1997**, *61*, 2779–2799. [CrossRef]

17. Stockwell, J.; Smith, L.; Jambor, J.L.; Beckie, R. The Relationship between Fluid Flow and Mineral Weathering in Heterogeneous Unsaturated Porous Media: A Physical and Geochemical Characterization of a Waste-Rock Pile. *Appl. Geochem.* **2006**, *21*, 1347–1361. [CrossRef]

18. Hochella, M.F., Jr.; Lower, S.K.; Maurice, P.A.; Penn, R.L.; Sahai, N.; Sparks, D.L.; Twining, B.S. Nanominerals, Mineral Nanoparticles, and Earth Systems. *Science* **2008**, *319*, 1631–1635. [CrossRef]

19. Hochella, M.F., Jr.; Mogk, D.W.; Ranville, J.; Allen, I.C.; Luther, G.W.; Marr, L.C.; McGrail, B.P.; Murayama, M.; Qafoku, N.P.; Rosso, K.M.; et al. Natural, Incidental, and Engineered Nanomaterials and Their Impacts on the Earth System. *Science* **2019**, *363*, eaau8299. [CrossRef]

20. Dolton, G.L.; Fox, J.E.; Clayton, J.L. *Petroleum Geology of the Powder River Basin, Wyoming and Montana*; Open-File Report, 88-450-P; U.S. Geological Survey: Reston, VA, USA, 1990. [CrossRef]

21. Flores, R.M. *Coalbed Methane in the Powder River Basin, Wyoming and Montana: An Assessment of the Tertiary-Upper Cretaceous Coalbed Methane Total Petroleum System*; Digital Data Series DDS–69–C; U.S. Geological Survey: Reston, VA, USA, 2004.

22. Fort Union Coal Assessment Team. *Resource Assessment of Selected Tertiary Coal Beds and Zones in the Northern Rocky Mountains and Great Plains Region*; Professional Paper 1625-A; U.S. Geological Survey: Reston, VA, USA, 1999. [CrossRef]

23. Yuretich, R.F.; Hickey, L.J.; Gregson, B.P.; Hsia, Y.L. Lacustrine Deposits in the Paleocene Fort Union Formation, Northern Bighorn Basin, Montana. *J. Sediment. Res.* **1984**, *54*, 836–852. [CrossRef]

24. Pocknall, D.T. Paleoenvironments and Age of the Wasatch Formation (Eocene), Powder River Basin, Wyoming. *PALAIOS* **1987**, *2*, 368–376. [CrossRef]

25. Lorenz, J.C.; Nadon, G.C. Braided-River Deposits in A Muddy Depositional Setting: The Molina Member of the Wasatch Formation (Paleogene), West-Central Colorado, U.S.A. *J. Sediment. Res.* **2002**, *72*, 376–385. [CrossRef]

26. Roehler, H.W. *Revised Stratigraphic Nomenclature for the Wasatch and Green River Formations of Eocene Age, Wyoming, Utah, and Colorado*; Professional Paper 1506-B; U.S. Geological Survey: Reston, VA, USA, 1991. [CrossRef]

27. Hoy, R.; Ogle, K.; Taylor, M. Evaluation of Water Quality Conditions in Coal Mine Backfill in the Powder River Basin of Wyoming. *J. Am. Soc. Min. Reclam.* **2003**, *2003*, 427–447. [CrossRef]

28. Belt, E.S.; Flores, R.M.; Warwick, P.D.; Conway, K.M.; Johnson, K.R.; Waskowitz, R.S. Relationship of Fluviodeltaic Facies to Coal Deposition in the Lower Fort Union Formation (Palaeocene), South-Western North Dakota. In *Sedimentology of Coal and Coal-Bearing Sequences*; Rahmani, R.A., Flores, R.M., Eds.; Wiley: Hoboken, NJ, USA, 1985. [CrossRef]

29. Ellis, M.S. *Quality of Economically Extractable Coal Beds in the Gillette Coal Field as Compared with Other Tertiary Coal Beds in the Powder River Basin, Wyoming and Montana*; Open-File Report 2002-174; U.S. Geological Survey: Reston, VA, USA, 2002. [CrossRef]

30. McClurg, J.E. Peat Forming Wetlands and the Thick Powder River Basin Coals; American Association of Petroleum Geologists, Eastern Powder River Basin—Black Hills. In Proceedings of the 39th Annual Field Conference Guidebook, Casper, WY, USA, 9–11 September 1988.

31. Moore, T.A. The Effects of Clastic Sedimentation on Organic Facies Development within a Tertiary Subbituminous Coal Bed, Powder River Basin, Montana, U.S.A. *Int. J. Coal Geol.* **1991**, *18*, 187–209. [CrossRef]

32. Palmer, C.A.; Mroczkowski, S.J.; Kolker, A.; Finkelman, R.B.; Bullock, J.H., Jr. *Chemical Analysis and Modes of Occurrence of Selected Trace Elements in a Powder River Basin Coal and Its Corresponding Simulated Cleaned Coal*; Open-File Report 2000-323; U.S. Geological Survey: Reston, VA, USA, 2001. [CrossRef]

33. Milligan, C.; Reddy, K. Monitoring of Groundwater Contamination by Trace Elements from CBNG Disposal Ponds Across the Powder River Basin, Wyoming. *J. Am. Soc. Min. Reclam.* **2007**, *2007*, 520–527. [CrossRef]

34. Wyoming State Engineer's Office. *Fort Union Formation Aquifer Monitoring Plan and Preliminary Aquifer Management Plan*; Wyoming Water Development Commission: Gillette, WY, USA, 1995; p. 73.

35. U.S. Environmental Protection Agency. *Method 1669, Sampling Ambient Water for Trace Metals at EPA Water Quality Criteria Levels*; USEPA Office of Water Engineering and Analysis Division: Washington, DC, USA, 1996; p. 35.

36. U.S. Geological Survey. National Field Manual for Collection of Water-Quality Data—Chapter A4. In *Collection of Water Samples*; U.S. Geological Survey: Reston, VA, USA, 2006; p. 231.

37. *ASTM D75/D75M-19*; Practice for Sampling Aggregates. ASTM International: West Conshohocken, PA, USA, 2019; p. 7. [CrossRef]

38. Lapakko, K.A.; White, W.W. Modification of the ASTM 5744-96 Kinetic Test. In Proceedings of the Fifth International Conference on Acid Rock Drainage; Society for Mining, Metallurgy, and Exploration: Littleton, CO, USA, 2000; pp. 631–639.

39. American Society for Testing and Materials. *Test Method for Laboratory Weathering of Solid Materials Using a Humidity Cell*; ASTM International: West Conshohocken, PA, USA, 2018; p. 24.

40. *ASTM D4644-04*; Test Method for Slake Durability of Shales and Similar Weak Rocks. ASTM International: West Conshohocken, PA, USA, 2010; p. 4. [CrossRef]

41. Fan, R.; Qian, G.; Li, Y.; Short, M.D.; Schumann, R.C.; Chen, M.; Smart, R.S.C.; Gerson, A.R. Evolution of Pyrite Oxidation from a 10-Year Kinetic Leach Study: Implications for Secondary Mineralisation in Acid Mine Drainage Control. *Chem. Geol.* **2022**, *588*, 120653. [CrossRef]

42. Kolker, A.; Palmer, C.A.; Bragg, L.J.; Bunnell, J.E. *Arsenic in Coal*; Fact Sheet 2005–3152; U.S. Geological Survey: Reston, VA, USA, 2005; p. 4.

43. Hagmaier, J.L. Groundwater Flow, Hydrochemistry, and Uranium Deposition in the Powder River Basin, Wyoming. Ph.D. Dissertation, University of North Dakota, Grand Forks, ND, USA, 1971.

44. Ayers, W.B., Jr. Lacustrine and Fluvial-Deltaic Depositional Systems, Fort Union Formation (Paleocene), Powder River Basin, Wyoming and Montana, American Association of Petroleum Geologists. *AAPG Bull.* **1986**, *70*, 1651–1673.

45. Harrison, A.L.; Dipple, G.M.; Song, W.; Power, I.M.; Mayer, K.U.; Beinlich, A.; Sinton, D. Changes in Mineral Reactivity Driven by Pore Fluid Mobility in Partially Wetted Porous Media. *Chem. Geol.* **2017**, *463*, 1–11. [CrossRef]

46. Nordstrom, D.K. Sulfide Mineral Oxidation. In *Encyclopedia of Geobiology*; Reitner, J., Thiel, V., Eds.; Encyclopedia of Earth Sciences Series; Springer: Dordrecht, The Netherlands, 2011; pp. 856–858. ISBN 978-1-4020-9211-4.

47. Carroll, D. *Rock Weathering*; Monographs in Geoscience; Springer: Greer, SC, USA, 1970; ISBN 978-1-4684-1796-8.

48. Finkelman, R.B.; Palmer, C.A.; Wang, P. Quantification of the Modes of Occurrence of 42 Elements in Coal. *Int. J. Coal Geol.* **2018**, *185*, 138–160. [CrossRef]

49. Finkelman, R. The Inorganic Geochemistry of Coal: A Scanning Electron Microscopy View. *Scanning Microsc.* **1987**, *21*, 9.

50. Sharp, W.N.; McKay, E.J.; McKeown, F.A.; White, A.M. *Geology and Uranium Deposits of the Pumpkin Buttes Area of the Powder River Basin, Wyoming*; Contributions to the Geology of Uranium; Bulletin 1107-H; U.S. Geological Survey: Reston, VA, USA, 1964. [CrossRef]

51. Luppens, J.A.; Scott, D.C.; Haacke, J.E.; Osmonson, L.M.; Rohrbacher, T.J.; Ellis, M.S. *Assessment of Coal Geology, Resources, and Reserves in the Gillette Coalfield, Powder River Basin, Wyoming*; Open-File Report 2008-1202; U.S. Geological Survey: Reston, VA, USA, 2008. [CrossRef]

52. Frascoli, F.; Hudson-Edwards, K.A. Geochemistry, Mineralogy and Microbiology of Molybdenum in Mining-Affected Environments. *Minerals* **2018**, *8*, 42. [CrossRef]

53. Horan, K. The Oxidative Weathering of Organic Matter and Its Carbon Dioxide Emissions: Insight from the Trace Elements Rhenium and Molybdenum. Ph.D. Dissertation, Durham University, Durham, UK, 2018.

54. Yudovich, Y.E.; Ketris, M.P. Selenium in Coal: A Review. *Int. J. Coal Geol.* **2006**, *67*, 112–126. [CrossRef]

55. Bao, Z.; Bain, J.; Saurette, E.; Zou Finfrock, Y.; Hu, Y.; Ptacek, C.J.; Blowes, D.W. Mineralogy-Dependent Sulfide Oxidation via Polysulfide and Thiosulfate Pathways during Weathering of Mixed-Sulfide Bearing Mine Waste Rock. *Geochim. Cosmochim. Acta* **2022**, *317*, 523–537. [CrossRef]

56. Dreher, G.B.; Finkelman, R.B. Selenium Mobilization in a Surface Coal Mine, Powder River Basin, Wyoming, U.S.A. *Environ. Geol. Water Sci.* **1992**, *19*, 155–167. [CrossRef]

57. Stillings, L.L.; Foster, A.L.; Koski, R.A.; Munk, L.; Shanks, W.C. Temporal Variation and the Effect of Rainfall on Metals Flux from the Historic Beatson Mine, Prince William Sound, Alaska, USA. *Appl. Geochem.* **2008**, *23*, 255–278. [CrossRef]

58. Wang, H.; Jiang, R.; Wang, B.; Yao, S. The Effect of Gypsum on the Fixation of Selenium in the Iron/Calcium-Selenium Coprecipitation Process. *Bull. Environ. Contam. Toxicol.* **2021**, *106*, 121–125. [CrossRef] [PubMed]

59. Lee, R.W. *Geochemistry of Water in the Fort Union Formation of the Northern Powder River Basin, Southeastern Montana*; Open-File Report; Open-File Report 80-336; U.S. Geological Survey: Reston, VA, USA, 1980. [CrossRef]

60. Huggins, F.E.; Huffman, G.P.; Lin, M.C. Observations on Low-Temperature Oxidation of Minerals in Bituminous Coals. *Int. J. Coal Geol.* **1983**, *3*, 157–182. [CrossRef]

61. See, R.B.; Reddy, K.J.; Vance, G.F.; Fadlelmawla, A.A.; Blaylock, M.J. *Geochemical Processes and the Effects of Natural Organic Solutes on the Solubility of Selenium in Coal-Mine Backfill Samples from the Powder River Basin, Wyoming*; Water-Resources Investigations Report 95-4200; U.S. Geological Survey: Reston, VA, USA, 1995. [CrossRef]

62. Healy, R.W.; Rice, C.A.; Bartos, T.T.; McKinley, M.P. Infiltration from an Impoundment for Coal-Bed Natural Gas, Powder River Basin, Wyoming: Evolution of Water and Sediment Chemistry. *Water Resour. Res.* **2008**, *44*. [CrossRef]

63. Rice, C.A.; Flores, R.M.; Stricker, G.D.; Ellis, M.S. Chemical and Stable Isotopic Evidence for Water/Rock Interaction and Biogenic Origin of Coalbed Methane, Fort Union Formation, Powder River Basin, Wyoming and Montana U.S.A. *Int. J. Coal Geol.* **2008**, *76*, 76–85. [CrossRef]

64. Elrashidi, M.A.; Adriano, D.C.; Workman, S.M.; Lindsay, W.L. Chemical Equilibria of Selenium in Soils: A Theoretical Development. *Soil Sci.* **1987**, *144*, 141–152. [CrossRef]

65. Paydary, P.; Schellenger, A.E.P.; Teli, M.; Jaisi, D.P.; Onnis-Hayden, A.; Larese-Casanova, P. Chemical Oxidation of Selenite to Selenate: Evaluation of Reactive Oxygen Species and O Transfer Pathways. *Chem. Geol.* **2021**, *575*, 120229. [CrossRef]

66. Torres, J.; Pintos, V.; Gonzatto, L.; Domínguez, S.; Kremer, C.; Kremer, E. Selenium Chemical Speciation in Natural Waters: Protonation and Complexation Behavior of Selenite and Selenate in the Presence of Environmentally Relevant Cations. *Chem. Geol.* **2011**, *288*, 32–38. [CrossRef]

67. Stoeppler, M. *Hazardous Metals in the Environment*; Techniques and Instrumentation in Analytical Chemistry; Elsevier Science: Amsterdam, The Netherlands, 1992; ISBN 978-0-08-087560-6.

68. Brownfield, M.E.; Cathcart, J.D.; Affolter, R.H.; Brownfield, I.K.; Rice, C.A.; O'Connor, J.T.; Zielinski, R.A.; Bullock, J.H.; Hower, J.C.; Meeker, G.P. *Characterization and Modes of Occurrence of Elements in Feed Coal and Coal Combustion Products from a Power Plant Utilizing Low-Sulfur Coal from the Powder River Basin, Wyoming*; Scientific Investigations Report 2004-5271; U.S. Geological Survey: Reston, VA, USA, 2005. [CrossRef]

69. Li, X.; Zhou, J.; Zhou, T.; Li, Z.; Hu, P.; Luo, Y.; Christie, P.; Wu, L. Potential Mobilization of Cadmium and Zinc in Soils Spiked with Smithsonite and Sphalerite under Different Water Management Regimes. *J. Environ. Manag.* **2022**, *324*, 116336. [CrossRef]

70. Acero, P.; Cama, J.; Ayora, C. Sphalerite Dissolution Kinetics in Acidic Environment. *Appl. Geochem.* **2007**, *22*, 1872–1883. [CrossRef]

71. Langman, J.B.; Moore, M.L.; Ptacek, C.J.; Smith, L.; Sego, D.; Blowes, D.W. Diavik Waste Rock Project: Evolution of Mineral Weathering, Element Release, and Acid Generation and Neutralization during a Five-Year Humidity Cell Experiment. *Minerals* **2014**, *4*, 257–278. [CrossRef]

72. Williamson, M.A.; Rimstidt, J.D. The Kinetics and Electrochemical Rate-Determining Step of Aqueous Pyrite Oxidation. *Geochim. Cosmochim. Acta* **1994**, *58*, 5443–5454. [CrossRef]

73. Hu, G.; Dam-Johansen, K.; Wedel, S.; Hansen, J.P. Decomposition and Oxidation of Pyrite. *Prog. Energy Combust. Sci.* **2006**, *32*, 295–314. [CrossRef]

74. Langman, J.B.; Blowes, D.W.; Veeramani, H.; Wilson, D.; Smith, L.; Sego, D.C.; Paktunc, D. The Mineral and Aqueous Phase Evolution of Sulfur and Nickel with Weathering of Pyrrhotite in a Low Sulfide, Granitic Waste Rock. *Chem. Geol.* **2015**, *401*, 169–179. [CrossRef]

75. Wunderly, M.D.; Blowes, D.W.; Frind, E.O.; Ptacek, C.J. Sulfide Mineral Oxidation and Subsequent Reactive Transport of Oxidation Products in Mine Tailings Impoundments: A Numerical Model. *Water Resour. Res.* **1996**, *32*, 3173–3187. [CrossRef]

76. Langman, J.B.; Ali, J.D.; Child, A.W.; Wilhelm, F.M.; Moberly, J.G. Sulfur Species, Bonding Environment, and Metal Mobilization in Mining-Impacted Lake Sediments: Column Experiments Replicating Seasonal Anoxia and Deposition of Algal Detritus. *Minerals* **2020**, *10*, 849. [CrossRef]

77. Dos Santos, E.C.; de Mendonça Silva, J.C.; Duarte, H.A. Pyrite Oxidation Mechanism by Oxygen in Aqueous Medium. *J. Phys. Chem. C* **2016**, *120*, 2760–2768. [CrossRef]

78. Lehmann, N.; Lantuit, H.; Böttcher, M.E.; Hartmann, J.; Eulenburg, A.; Thomas, H. Alkalinity Generation from Carbonate Weathering in a Silicate-Dominated Headwater Catchment at Iskorasfjellet, Northern Norway. *Biogeosciences* **2023**, *20*, 3459–3479. [CrossRef]

79. Agbenin, J.O.; van Raij, B. Rate Processes of Calcium, Magnesium and Potassium Desorption from Variable-Charge Soils by Mixed Ion-Exchange Resins. *Geoderma* **1999**, *93*, 141–157. [CrossRef]

80. White, A.F.; Blum, A.E.; Schulz, M.S.; Bullen, T.D.; Harden, J.W.; Peterson, M.L. Chemical Weathering Rates of a Soil Chronosequence on Granitic Alluvium: I. Quantification of Mineralogical and Surface Area Changes and Calculation of Primary Silicate Reaction Rates. *Geochim. Cosmochim. Acta* **1996**, *60*, 2533–2550. [CrossRef]

81. Skorina, T.; Allanore, A. Aqueous Alteration of Potassium-Bearing Aluminosilicate Minerals: From Mechanism to Processing. *Green Chem.* **2015**, *17*, 2123–2136. [CrossRef]

82. Sparks, D.L. Chemical Kinetics and Mass Transfer Processes in Soils and Soil Constituents. In *Transport Processes in Porous Media*; Bear, J., Corapcioglu, M.Y., Eds.; NATO ASI Series; Springer: Dordrecht, The Netherlands, 1991; pp. 583–637. ISBN 978-94-011-3628-0.

83. Hem, J.D.; Cropper, W.H. *Survey of Ferrous-Ferric Chemical Equilibria and Redox Potentials*; Water Supply Paper; Water Supply Paper 1459-A; U.S. Geological Survey: Reston, VA, USA, 1959. [CrossRef]

84. Schwertmann, U. Solubility and Dissolution of Iron Oxides. *Plant Soil* **1991**, *130*, 1–25. [CrossRef]

85. Liang, L.; Morgan, J.J. Chemical Aspects of Iron Oxide Coagulation in Water: Laboratory Studies and Implications for Natural Systems. *Aquat. Sci.* **1990**, *52*, 32–55. [CrossRef]

86. Davison, W. Iron and Manganese in Lakes. *Earth-Sci. Rev.* **1993**, *34*, 119–163. [CrossRef]

87. Perret, D.; Gaillard, J.-F.; Dominik, J.; Atteia, O. The Diversity of Natural Hydrous Iron Oxides. *Environ. Sci. Technol.* **2000**, *34*, 3540–3546. [CrossRef]

88. Gaffney, J.W.; White, K.N.; Boult, S. Oxidation State and Size of Fe Controlled by Organic Matter in Natural Waters. *Environ. Sci. Technol.* **2008**, *42*, 3575–3581. [CrossRef]

89. Hassellöv, M.; Kammer, F. von der Iron Oxides as Geochemical Nanovectors for Metal Transport in Soil-River Systems. *Elements* **2008**, *4*, 401–406. [CrossRef]

90. Weber, F.-A.; Hofacker, A.F.; Voegelin, A.; Kretzschmar, R. Temperature Dependence and Coupling of Iron and Arsenic Reduction and Release during Flooding of a Contaminated Soil. *Environ. Sci. Technol.* **2010**, *44*, 116–122. [CrossRef]

91. Hatje, V.; Payne, T.E.; Hill, D.M.; McOrist, G.; Birch, G.F.; Szymczak, R. Kinetics of Trace Element Uptake and Release by Particles in Estuarine Waters: Effects of pH, Salinity, and Particle Loading. *Environ. Int.* **2003**, *29*, 619–629. [CrossRef]

92. Possemiers, M.; Huysmans, M.; Anibas, C.; Batelaan, O.; Van Steenwinkel, J. Reactive Transport Modeling of Redox Processes to Assess Fe(OH)$_3$ Precipitation around Aquifer Thermal Energy Storage Wells in Phreatic Aquifers. *Environ. Earth Sci.* **2016**, *75*, 648. [CrossRef]

93. Sun, H.; Chen, M.; Zou, L.; Shu, R.; Ruan, R. Study of the Kinetics of Pyrite Oxidation under Controlled Redox Potential. *Hydrometallurgy* **2015**, *155*, 13–19. [CrossRef]

94. Journet, E.; Desboeufs, K.V.; Caquineau, S.; Colin, J.-L. Mineralogy as a Critical Factor of Dust Iron Solubility. *Geophys. Res. Lett.* **2008**, *35*. [CrossRef]

95. Wang, Z.; Li, R.; Cui, L.; Fu, H.; Lin, J.; Chen, J. Characterization and Acid-Mobilization Study for Typical Iron-Bearing Clay Mineral. *J. Environ. Sci.* **2018**, *71*, 222–232. [CrossRef]